



Supplement of

Maximum ozone concentrations in the southwestern US and Texas: implications of the growing predominance of the background contribution

David D. Parrish et al.

Correspondence to: David D. Parrish (david.d.parrish.llc@gmail.com)

The copyright of individual parts of the supplement might differ from the article licence.

1 **Contents of this file**

2

3 Tables S1 to S8

4 Figures S1 to S8

5 Text S1 to S6

6

7

8 **Introduction**

9 This supporting information collects the parameter values derived from fits of Equations 3 and 4 to all ODV time
10 series analyzed in this work in Tables S1 to S5. Figures S1 to S6 illustrate some of these fits and provide additional
11 data presentations. Text S1 discusses the uncertainty of observation-based and chemical transport model results, and
12 Text S2 to S6 discuss additional issues that may affect the accuracy of the observation-based model.

13 **Table S1.** Parameter values (with 95% confidence limits) derived from fits of Equation 1 to time series of ODVs time
 14 series from the isolated rural CASTNET sites.

Site	a (ppb)	b (ppb yr ⁻¹)	c (ppb yr ⁻²)	year _{max}	RMSD (ppb)
Glacier NP	54.9 ± 1.1	0.09 ± 0.16	-0.010 ± 0.011	2004 ± 9	1.2
Yellowstone NP	65.9 ± 2.9	-0.31 ± 0.67	+0.007 ± 0.032	---	1.7
Craters of the Moon NM	62.5 ± 3.8	0.16 ± 0.67	-0.009 ± 0.038	2009 ± 51	2.4
Lassen Volcanic NP	72.4 ± 2.7	-0.05 ± 0.35	-0.016 ± 0.025	1999 ± 11	3.1
Great Basin NP	71.5 ± 2.1	0.14 ± 0.51	-0.020 ± 0.028	2004 ± 13	2.0
Canyonlands NP	70.3 ± 2.0	0.17 ± 0.46	-0.024 ± 0.024	2003 ± 10	1.7
Grand Canyon NP	72.5 ± 1.3	0.07 ± 0.21	-0.026 ± 0.014	2001 ± 4	1.4
Chiricahua NM	70.1 ± 1.7	0.19 ± 0.29	-0.020 ± 0.018	2005 ± 8	1.8
All sites	67.7 ± 1.9	0.09 ± 0.33	-0.018 ± 0.020	2003 ± 10	5.9
All sites - normalized	71.3 ± 0.8	0.07 ± 0.13	-0.015 ± 0.008	2002 ± 4	2.4

15

16

17 **Table S2.** Parameter values from fits of Equation 3 to time series of percentiles of maximum MDA8 ozone
 18 concentration distributions in the CA air basins and calculated from the ozone sondes launched from Trinidad Head
 19 CA. The 98th percentile is not included in Figure 2 of the paper, but is included here as it approximates the ODV.
 20 RMSD gives the root-mean-square deviations between the observed ozone concentrations and the derived fits.

Data set	<i>a</i> (ppb)	<i>A</i> (ppb)	RMSD (ppb)
Maximum			
San Diego AB	52.6 ± 13.4	58.6 ± 9.7	16.8
SoCAB	66.6 ± 13.4	95.8 ± 9.7	16.7
SFB AB	75.5 ± 9.6	25.1 ± 6.9	11.9
North Coast AB	65.4 ± 7.7	4.6 ± 6.0	12.0
Ozone sondes	76.5	---	---
98th percentile			
San Diego AB	58.6 ± 5.7	41.0 ± 4.1	7.1
SoCAB	60.8 ± 8.9	87.7 ± 6.4	11.1
SFB AB	70.2 ± 6.5	21.1 ± 4.7	8.0
North Coast AB	58.1 ± 5.7	4.3 ± 4.5	8.9
Ozone sondes	76.5	---	---
90th percentile			
San Diego AB	54.2 ± 3.5	32.5 ± 2.5	4.4
SoCAB	53.0 ± 5.6	76.6 ± 4.1	7.0
SFB AB	54.8 ± 5.1	18.5 ± 3.7	6.3
North Coast AB	47.6 ± 3.9	4.1 ± 3.0	6.1
Ozone sondes	52.3	---	---
75th percentile			
San Diego AB	49.5 ± 2.9	27.9 ± 2.1	3.7
SoCAB	50.0 ± 5.7	65.0 ± 4.1	7.1
SFB AB	45.6 ± 3.5	14.4 ± 2.5	4.3
North Coast AB	42.4 ± 3.2	3.0 ± 2.5	5.0
Ozone sondes	45.8	---	---
median			
San Diego AB	45.8 ± 3.0	21.5 ± 2.2	3.7
SoCAB	46.4 ± 5.9	50.8 ± 4.3	7.4
SFB AB	38.8 ± 2.8	10.9 ± 2.0	3.5
North Coast AB	37.6 ± 2.7	1.3 ± 2.1	4.2
Ozone sondes	39.3	---	---
25th percentile			
San Diego AB	43.2 ± 3.2	14.9 ± 2.3	4.0
SoCAB	45.6 ± 7.1	34.4 ± 5.1	8.8
SFB AB	33.8 ± 2.1	8.6 ± 1.5	2.6
North Coast AB	33.1 ± 2.7	0.5 ± 2.1	4.2
Ozone sondes	31.8	---	---
10th percentile			
San Diego AB	40.4 ± 2.8	10.1 ± 2.0	3.5
SoCAB	46.1 ± 6.9	18.0 ± 5.0	8.6
SFB AB	29.1 ± 2.0	7.7 ± 1.4	2.5
North Coast AB	29.3 ± 2.4	-0.7 ± 1.9	3.7
Ozone sondes	25.7	---	---
Minimum			
San Diego AB	31.5 ± 4.1	4.4 ± 3.2	6.4
SoCAB	43.1 ± 4.4	0.1 ± 3.4	6.9
SFB AB	22.7 ± 3.0	5.2 ± 2.4	4.7
North Coast AB	20.7 ± 3.3	-2.8 ± 2.6	5.1
Ozone sondes	5.8	---	---

22 **Table S3.** Parameter values from all fits of Equation 3 to time series of ODVs recorded in the southwestern US.
 23 RMSD gives the root-mean-square deviations between the observed ODVs and the derived fits.

Site(s)	a (ppb)	A (ppb)	Npts ^a	RMSD (ppb)	years
CASTNET					
CASTNET - normalized	68.5 ± 1.5	2.8 ± 1.9	212	2.3	1990-2021
Southwestern US - rural					
AZ rural	66.6 ± 1.9	5.4 ± 2.5	116	2.3	1990-2021
Southern UT, Mesquite NV	64.8 ± 3.6	6.5 ± 5.6	66	2.6	1995-2021
Four Corners area rural	69.6 ± 4.3	-2.7 ± 6.6	126	4.0	1996-2021
Southern NM rural	69.4 ± 5.5	-1.3 ± 8.0	76	4.7	1992-2021
CO rural	69.0 ± 3.1	-1.9 ± 4.4	97	4.0	1986-2021
Southwestern US - urban					
Phoenix	69.0 ± 1.7	9.4 ± 2.3	658	4.8	1990-2021
Phoenix max	75.2 ± 4.9	10.2 ± 5.4	32	2.9	1990-2021
Tucson	63.9 ± 1.4	7.5 ± 1.2	264	3.4	1975-2021
Tucson max	66.2 ± 2.9	9.7 ± 2.4	38	2.3	1980-2021
Las Vegas	68.0 ± 2.6	11.6 ± 3.8	230	3.1	2000-2021
Las Vegas max	69.6 ± 6.6	15.4 ± 9.9	22	2.3	2000-2021
Reno	66.3 ± 2.2	4.9 ± 2.4	169	3.8	1982-2021
Reno max	67.1 ± 4.8	6.8 ± 4.1	39	3.8	1982-2021
Salt Lake City	66.6 ± 1.9	11.8 ± 1.7	351	5.2	1977-2021
Salt Lake City max	68.9 ± 4.3	15.0 ± 3.2	43	3.8	1979-2021
Albuquerque-Santa Fe	66.2 ± 1.8	4.0 ± 1.7	275	3.8	1981-2021
Albuquerque-Santa Fe max	68.4 ± 3.0	5.3 ± 2.4	41	2.5	1981-2021
Denver	69.0 ± 2.1	8.0 ± 1.7	412	6.2	1974-2021
Denver max	74.7 ± 2.1	9.4 ± 1.4	47	4.3	1974-2021

24 ^a Npts gives the number of ODVs included in each fit

25

26

27

28 **Table S4.** Parameter values from fits of Equation 4 to time series of maximum ODVs recorded in southwestern US,
 29 Texas and two other urban areas, TX, New York City, with the a parameter held at that derived for all ODVs in the
 30 respective urban area. RMSD gives the root-mean-square deviations between the observed maximum ODVs and the
 31 derived fits.

Site(s)	a (ppb)	A_{WF} (ppb)	WF (ppb)	RMSD (ppb)	years
Southwestern US - urban					
Phoenix max	69.0	12.9 ± 3.6	1.6 ± 2.5	3.0	1990-2021
Tucson max	63.9	10.5 ± 1.6	1.4 ± 1.6	2.2	1980-2021
Las Vegas max	68.0	16.1 ± 6.6	0.8 ± 3.3	1.8	2000-2021
Reno max	66.3	7.0 ± 1.3	0.6 ± 1.4	3.8	1982-2021
Salt Lake City max	66.6	15.6 ± 2.0	1.6 ± 2.5	3.7	1977-2021
Albuquerque-Santa Fe max	66.2	6.0 ± 1.5	1.4 ± 1.7	2.5	1981-2021
Denver max	69.0	11.0 ± 1.7	4.0 ± 2.5	4.0	1974-2021
Other urban areas					
Houston max	53.9	54.4 ± 3.2	1.8 ± 2.0	3.6	1995-2021
Dallas max	57.7	43.0 ± 2.5	2.6 ± 1.2	1.7	2000-2021
El Paso max	64.6	14.2 ± 2.1	3.2 ± 2.8	4.3	1977-2021
New York City max	52.2	39.7 ± 2.3	3.1 ± 1.2	3.7	2000-2021
Atlanta max	49.1	54.4 ± 9.9	1.2 ± 6.1	5.4	1995-2021

32

33

34 **Table S5.** Parameter values from all fits of Equation 3 to time series of ODVs recorded in nine Texas regions and
 35 neighboring states. RMSD gives the root-mean-square deviations between the observed ODVs and the derived fits.

Site(s)	a (ppb)	A (ppb)	Npts ^a	RMSD (ppb)	years
CASTNET					
CASTNET - normalized	68.5 ± 1.5	2.8 ± 1.9	212	2.3	1990-2021
Texas Regions					
Dallas region	57.7 ± 3.1	34.6 ± 4.5	422	5.9	1995-2021
Houston region	53.9 ± 3.2	43.2 ± 4.2	478	6.7	1995-2021
El Paso region	64.6 ± 1.8	11.5 ± 1.7	366	4.9	1976-2021
San Antonio region	58.4 ± 4.1	26.6 ± 6.3	138	3.9	2000-2021
Beaumont-PA-LC	54.7 ± 3.4	28.0 ± 5.1	230	4.0	2000-2021
So Coast Texas	52.1 ± 4.1	27.5 ± 6.0	63	2.5	2000-2021
SW Texas	49.8 ± 4.9	18.2 ± 6.9	72	3.1	2000-2021
Tyler-LV-SP	50.8 ± 4.6	37.3 ± 6.8	89	3.5	2000-2021
Western rural region	64.9 ± 5.8	3.2 ± 8.1	50	3.5	1989-2017
Other Western States					
Oklahoma	56.6 ± 2.8	25.1 ± 4.4	365	4.0	2000-2021
Louisiana	54.3 ± 2.3	29.9 ± 3.3	519	4.2	2000-2021
Arkansas	48.2 ± 4.7	37.5 ± 7.6	141	4.5	2000-2021
Kansas	56.6 ± 4.2	20.2 ± 6.6	174	4.3	2000-2021
Nebraska	56.5 ± 4.0	7.4 ± 3.6	146	6.6	1980-2021
Montana	58.6 ± 1.6	1.25 ^b	99	4.7	1979-2021
North Dakota	59.6 ± 0.9	1.25 ^b	181	3.6	1982-2021
South Dakota	62.2 ± 1.7	1.25 ^b	80	4.4	1990-2021
Wyoming	64.2 ± 0.6	1.25 ^b	227	2.8	1999-2021

36 ^a Npts gives the number of ODVs included in each fit

37 ^b Fit with A parameter value held fixed at this value

38

39

40

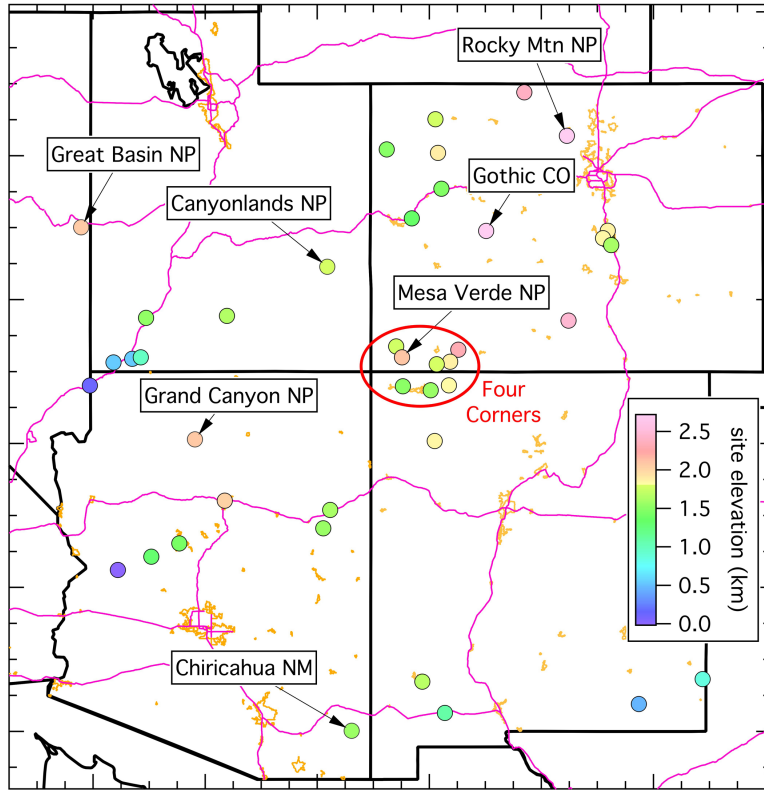
41

42

43 **Table S6.** Two-letter state abbreviations

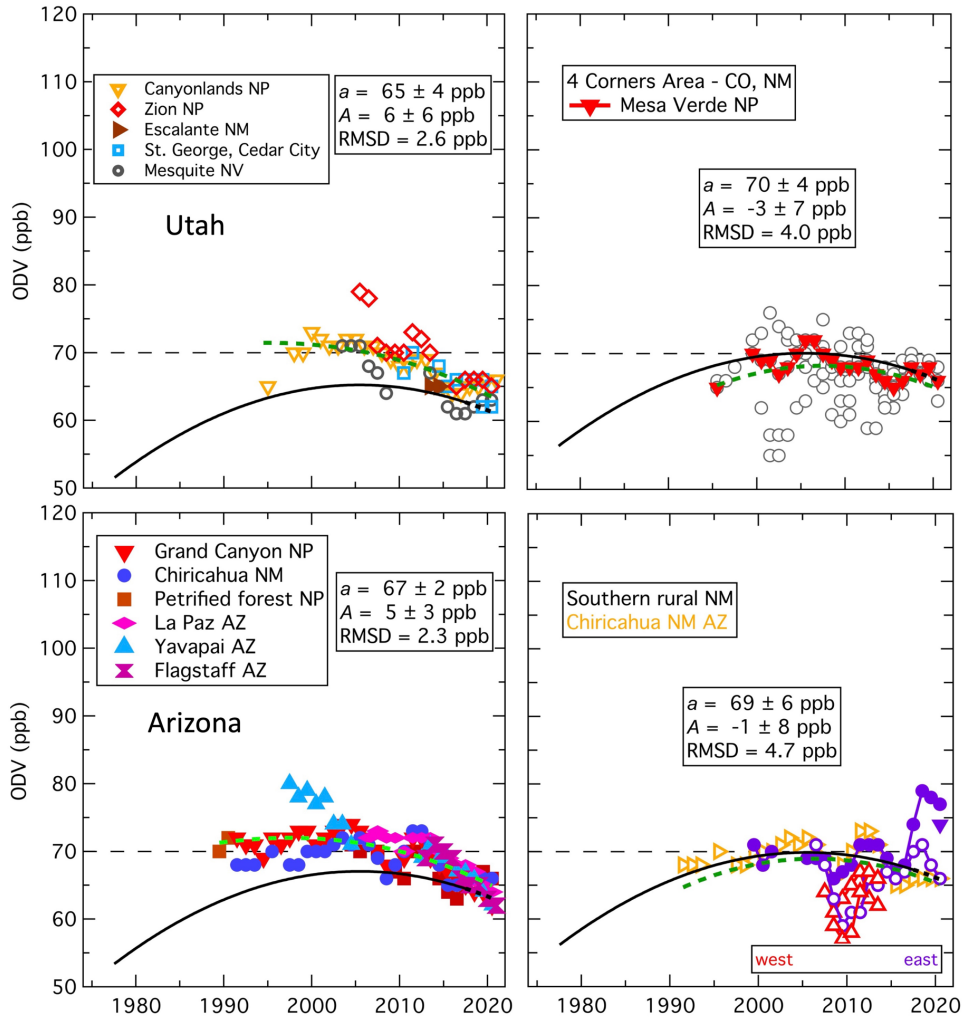
State		State		State	
Alabama	AL	Kentucky	KY	North Dakota	ND
Alaska	AK	Louisiana	LA	Ohio	OH
Arizona	AZ	Maine	ME	Oklahoma	OK
Arkansas	AR	Maryland	MD	Oregon	OR
California	CA	Massachusetts	MA	Pennsylvania	PA
Colorado	CO	Michigan	MI	Rhode Island	RI
Connecticut	CT	Minnesota	MN	South Carolina	SC
Delaware	DE	Mississippi	MS	South Dakota	SD
District of Columbia	DC	Missouri	MO	Tennessee	TN
Florida	FL	Montana	MT	Texas	TX
Georgia	GA	Nebraska	NE	Utah	UT
Hawaii	HI	Nevada	NV	Vermont	VT
Idaho	ID	New Hampshire	NH	Virginia	VA
Illinois	IL	New Jersey	NJ	Washington	WA
Indiana	IN	New Mexico	NM	West Virginia	WV
Iowa	IA	New York	NY	Wisconsin	WI
Kansas	KS	North Carolina	NC	Wyoming	WY

44



45

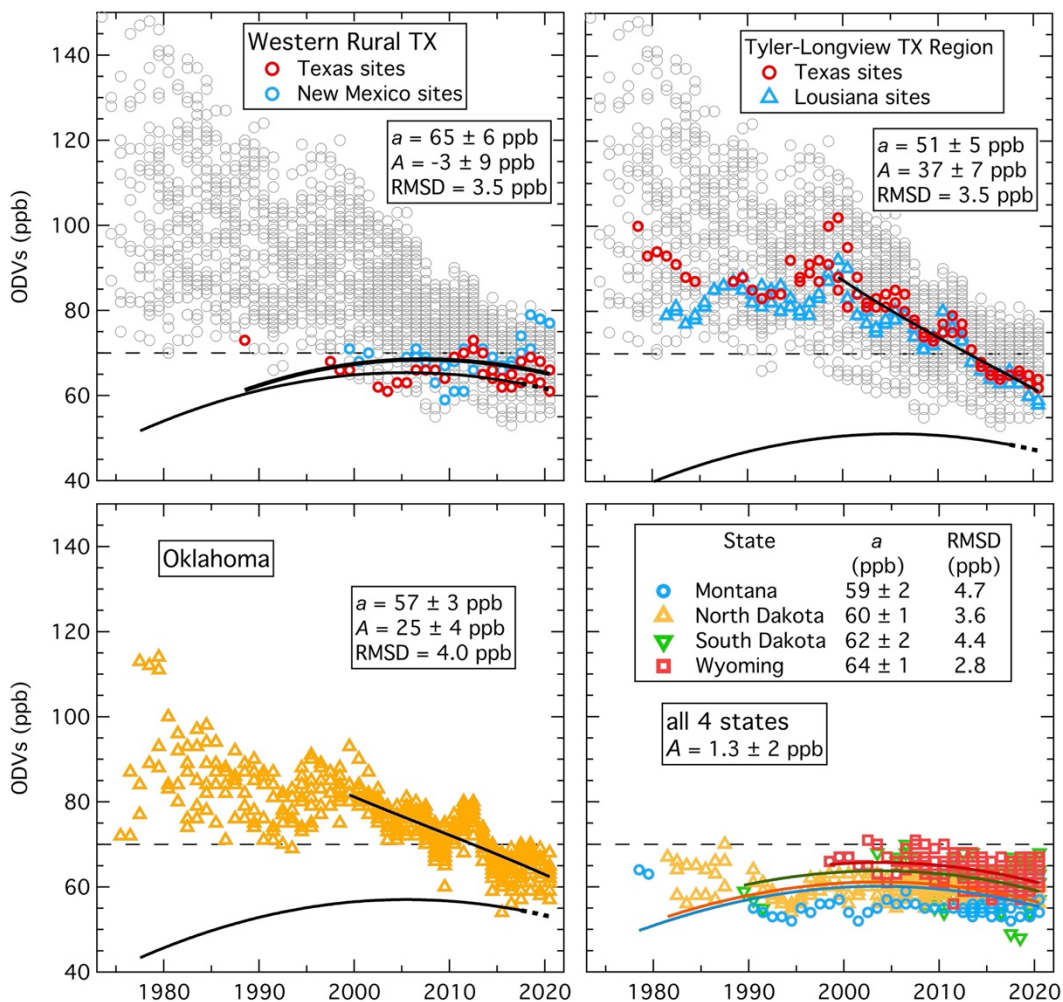
46 **Figure S1.** Map of southwestern US rural monitoring sites; the symbols are color-coded according to site elevation as
 47 annotated. Lines indicate outlines of southwestern US states (black), urban areas (gold) and interstates and selected
 48 other major highways (violet). ODV time series from rural areas whose sites are analyzed together as separate data
 49 sets are included in Figure S2. Locations of specific CASTNET sites as well as the Four Corners area are annotated.



50

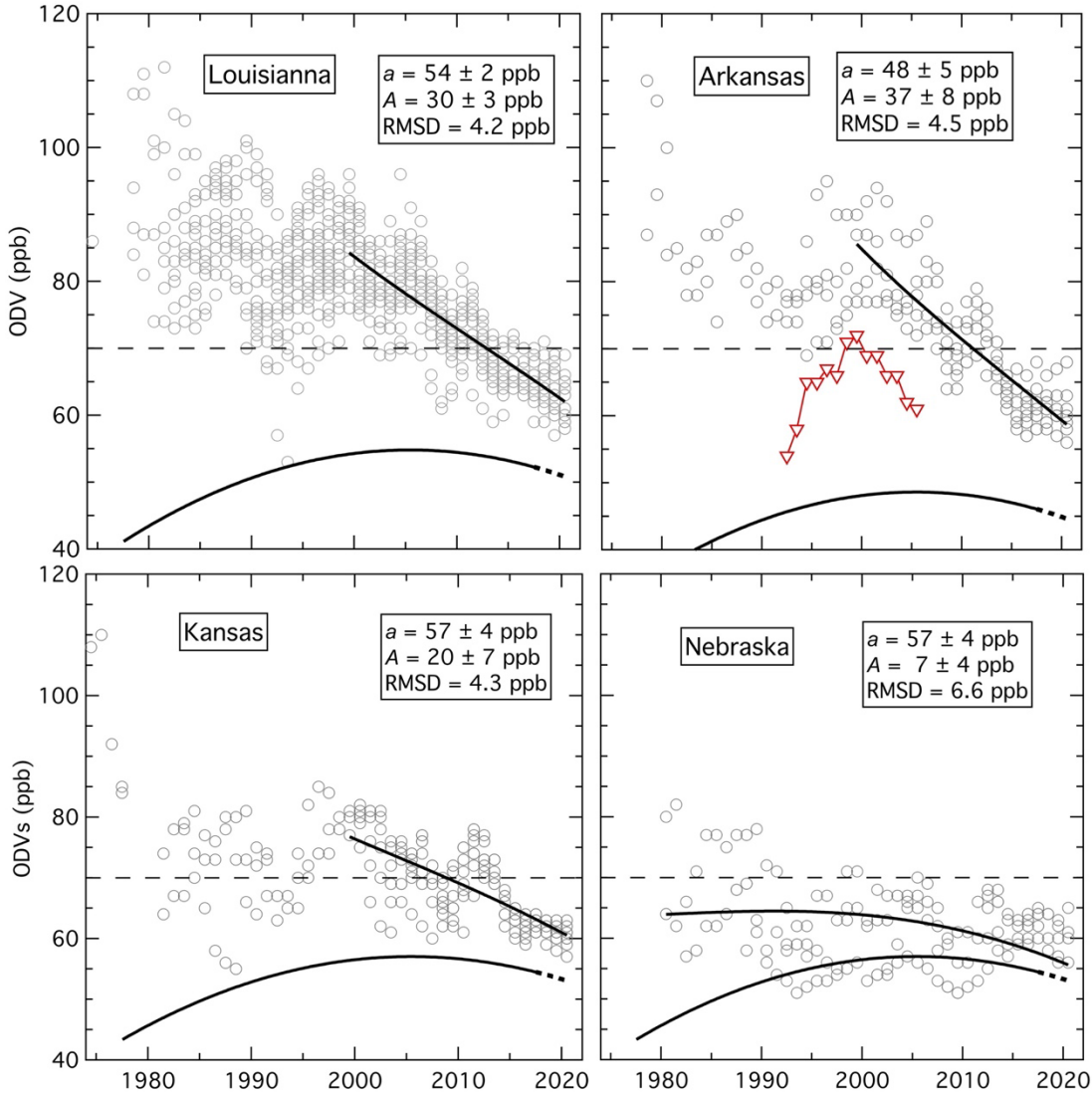
51
52
53
54
55

Figure S2. Time series of ODVs recorded in four southwestern US rural areas shown in Figure S1. Symbols indicate different sites as annotated. The southern NM sites are identified as western and eastern by different colors. Green dashed curves indicate fits of Equation 3 to all ODVs, with the parameters derived in the fit annotated. The black solid curves with dashed extensions indicate the fit to the baseline data from Figure 1, normalized to the respective a parameter values. The light dashed lines indicate the 70 ppb ozone NAAQS.



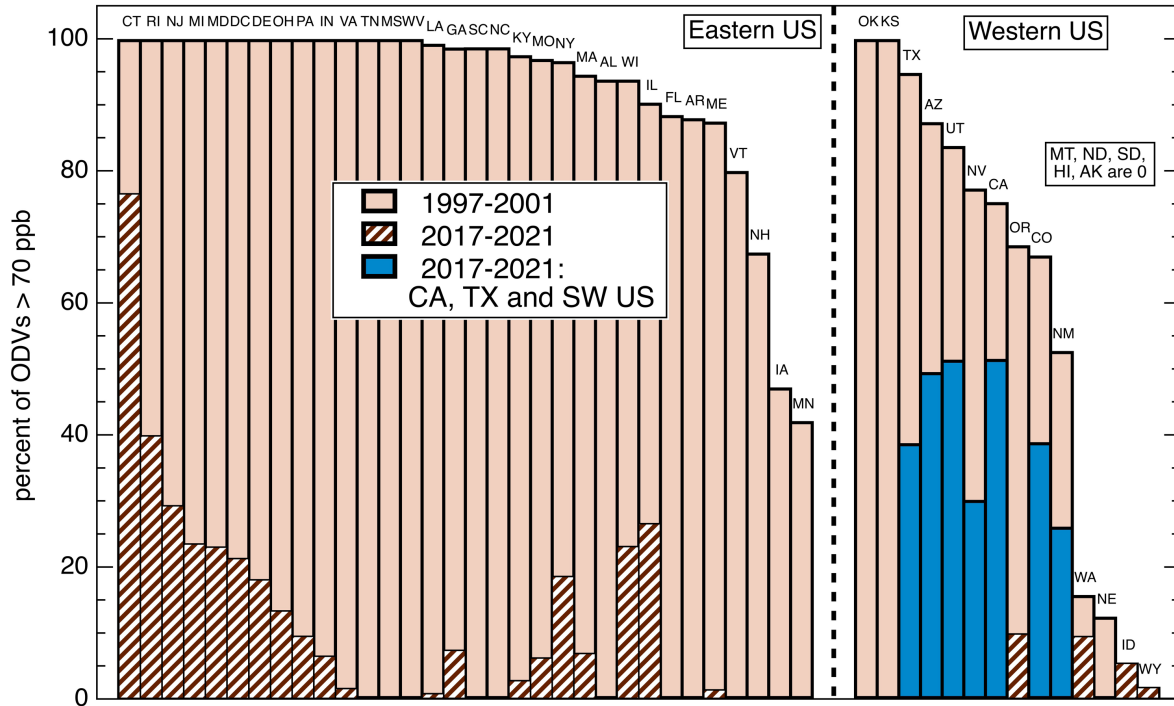
56

57 **Figure S3. (upper graphs)** Time series of ODVs recorded in two of the Texas regions shown in Figure 7 of the
 58 manuscript. Grey symbols in each graph indicate all recorded Texas ODVs. Colored symbols indicate the ODVs
 59 from each respective area. Upper curves indicate fits of Equation 3 to all ODVs in the area; the parameters derived
 60 in these fits are annotated. Lower curves with dashed extensions indicate the fit to the baseline data from Figure
 61 1, but here normalized to the respective a parameter values. **(lower graphs)** Time series of ODVs recorded in
 62 Oklahoma and the four northern rural states. For Oklahoma upper curve indicates fit of Equation 3 to all ODVs
 63 in the state for 2000-2021; the parameters derived in this fit is annotated. Lower curve with dashed extension
 64 indicates the fit to the baseline data from Figure 1, normalized to the a parameter value derived for Oklahoma. For
 65 the northern states the curves indicate fits of Equation 3 to all ODVs recorded in each state; in these fits the A
 66 parameter value is fixed at 1.25 ppb. The derived a parameter values are annotated. In all graphs, the light dashed
 67 lines indicate the 70 ppb ozone NAAQS.



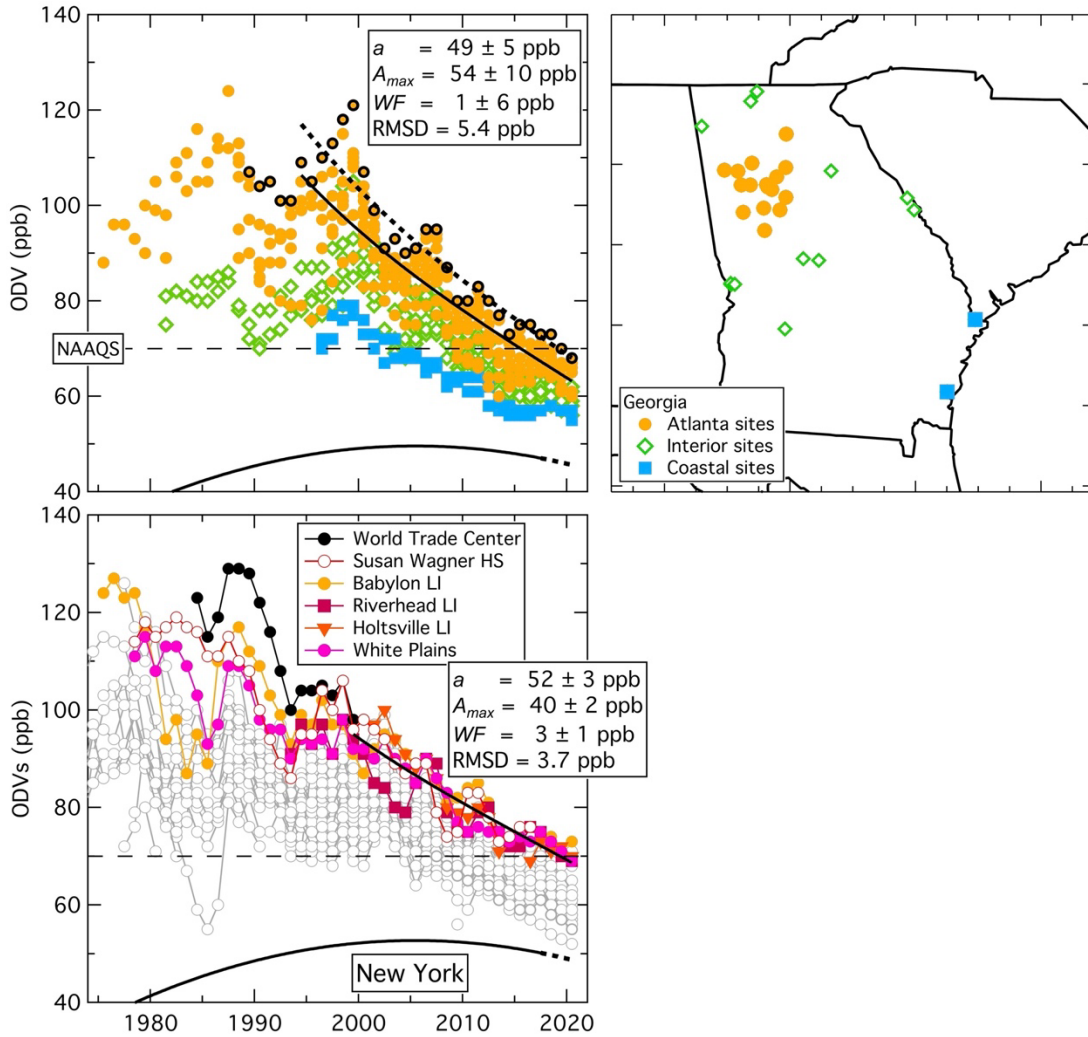
68

69 **Figure S4.** Analysis of time series of ODVs recorded in four neighboring states. Grey symbols in each graph indicate
70 all recorded ODVs in the states. Upper curves indicate fits of Equation 3 to all ODVs in the respective states. The
71 parameters derived in these fits are annotated. Lower curves with dashed extensions indicate the fit to the baseline
72 data from Figure 1, normalized to the respective a parameter values. Colored symbols in Arkansas indicate the ODVs
73 from a single site that appear to be outliers, and are excluded from the fit.



74

75 **Figure S5.** Comparison of percentage of ODVs greater than 70 ppb recorded at all sites in individual states over two
 76 5-year periods: 2017-2021 (hatched and dark blue bars) and a period 20 years earlier - 1997-2001 (light-colored bars).
 77 Individual states are indicated by their two letter abbreviations (defined in Table S6). States are arbitrarily divided
 78 between eastern and western regions. Southwestern states, Texas and California are indicated by solid dark blue bars.
 79 Five states, all in the western region, reported no ODVs greater than 70 ppb. Format is the same as Figure 9 of the
 80 manuscript.



81

82 **Figure S6.** Analysis of time series of ODVs recorded in two eastern urban areas – Atlanta GA and New York City
 83 NY. In Georgia ODVs from three groups of sites are indicated with different symbols. Grey symbols in lower graph
 84 indicate all recorded ODVs in NY. In the GA graph, upper solid curve indicates fit of Equation 3 to all Atlanta ODVs
 85 and the dotted curve indicates fit of Equation 4 to maximum Atlanta ODVs indicated by outlined circles. In NY graph,
 86 upper solid curve indicates fit of Equation 4 to the ODVs recorded at the sites representing the maxima in New York
 87 City. The parameters derived in the fits to Equation 4 are annotated. Lower curves with dashed extensions indicate
 88 the fit to the baseline data from Figure 1, normalized to the respective a parameter values. The light dashed lines
 89 indicate the 70 ppb ozone NAAQS.

90

91 S1. Uncertainty of observation-based and chemical transport model results

92 Equation 3 provides excellent fits to long-term ozone changes in diverse US regions. As written, Equation 3 has 5
93 adjustable parameters (a , b , c , A , τ); however 3 of these are constants whose values have been determined in previous
94 analyses. Parrish et al. (2020) determined values for $b = 0.20 \pm 0.06$ ppb yr⁻¹ and $c = 0.018 \pm 0.006$ ppb yr⁻² that were
95 the same within derived confidence limits throughout northern midlatitudes. Parrish et al. (2021a) show that these
96 results are consistent with results from 28 published quantifications of changes in average surface ozone
97 concentrations at remote and rural western US locations that are thought to represent background ozone transported
98 into North America. Parrish et al. (2017; 2022) determined a value of $\tau = 21.8 \pm 0.8$ years from the time dependence
99 of ODVs in 7 southern California air basins. This same value (within confidence limits) fit ODV time series throughout
100 the western and northern US (Parrish et al., 2022) and in the northeastern US (Parrish and Ennis, 2019). Substitution
101 of these values for b , c and τ into Equation 3 leaves only 2 unknown parameters: a and A . Section 4 of the paper shows
102 that the resulting Equation 3 with varying a and A parameter values provides excellent fits to all percentiles of the
103 distributions of the maximum MDA8 ozone concentrations in 4 urban and rural California air basins (Figure 2), and
104 also to ODV time series recorded at rural and remote western US CASTNET sites (Figure 1), at urban and rural sites
105 throughout the southwestern US and Texas (Figures 5, 6 and 8), and in surrounding and more distant US states (Figures
106 S2-S4 and S6). Previous work (Parrish et al, 2017; 2022; Parrish and Ennis, 2019) demonstrate that same equation (or
107 one closely related) provides excellent fits to ODV time series recorded urban and rural sites along the entire US West
108 Coast, in the northern rural states and in the northeastern US.

109 It is widely accepted that photochemical ozone production involves a very complex set of physical and chemical
110 processes, and that complexity causes ambient ozone concentrations to exhibit a highly non-linear dependence upon
111 precursor concentrations (see e.g., Monks et al., 2015). The excellent fits of a 2 parameter equation to a great number
112 of long-term ozone concentration time series recorded in a widely diverse range of environments demonstrates that
113 there is an underlying simplicity to the evolution of ozone concentrations throughout the US, notwithstanding the
114 complexity of ozone photochemistry. Fully understanding the origins of this simplicity may provide a very useful
115 challenge for CTMs studies.

116 In previous papers we have discussed inconsistencies between results of observation-based and chemical transport
117 model (CTM) simulations, and among results from different CTM simulations. Section 3.4 and Figure 6 of Parrish et
118 al. (2017) show seven CTM-derived US background ODV estimates for southern California air basins that varied
119 from ~45 to ~65 ppb, with one outlier of 92 ppb; the observational-derived value of 62 ppb agrees well with one of
120 those model results, although it is larger than most others. In their Section 4.2 Parrish and Ennis (2019) compare
121 results from three CTMs with those from our observational-based approach in five US regions; these comparisons
122 show significant spatial correlation between approaches (r^2 values for different CTMs with the observational-based
123 results vary from 0.31 to 0.90), but the CTMs are, on average, systematically lower by 4 to 13 ppb. Zhang et al. (2020)
124 find disagreements of similar magnitude between CTMs; US background ozone estimates from two state-of-the-art
125 global models differed by 5 ppb on average and up to 15 ppb episodically. These disagreements have led to the
126 increasing recognition that CTMs are not yet able to provide accurate estimates of atmospheric ozone concentrations

127 without incorporating additional information from observations; see, e.g., Skipper et al. (2021) and Hosseinpour et al.
 128 (2024).

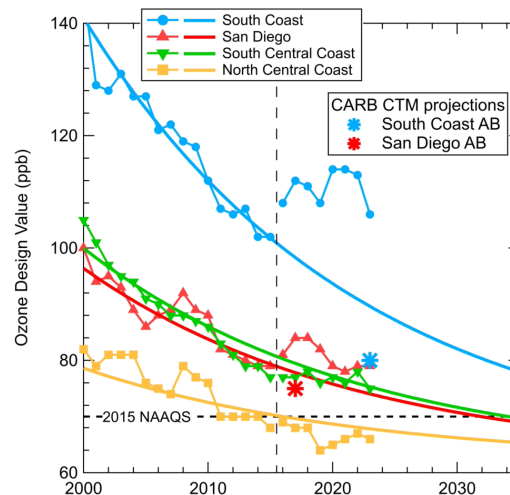
129 The results of Hosseinpour et al. (2024) are particularly relevant to the present paper. The authors used a random
 130 forest machine learning algorithm to improve CTM estimates of US background ozone extreme values (4th largest
 131 MDA8, i.e., comparable to our US background ODV) in four of the urban areas considered in our analysis (Table S7).
 132 The original CTM results were lower than the results derived in the present paper from the observation-based model
 133 by an average of 14 ppb for the three SW US urban areas, and 5 ppb for Houston; after correction the CTM results
 134 were increased so that they were lower by only 2 or 3 ppb in all four cities. In the end, the machine learning
 135 algorithm had forced the CTM to match the observations, so that the CTM was no longer a free running simulation of
 136 the relevant physical and chemical processes. Instead, the combination of the CTM and the machine learning algorithm
 137 constituted an elaborate observational-based model. It is encouraging that this alternative observational-based
 138 approach gave results similar to those derived in this work from our much simpler observational-based model.

139 **Table S7.** CAMx simulated 4th highest MDA8 background ozone concentration over April through September 2016
 140 before and after adjustment by the random forest algorithm reported (Hosseinpour et al., 2024) compared to our
 141 results for US background ODV in 2016. (Units: ppb)

	Phoenix	Salt Lake City	Denver	Houston
CAMx original simulation (Hosseinpour et al. table 3)	52	51	54	48
Random Forest adjusted CTM (Hosseinpour et al. table 8)	66	63	65	50
US background ODV (this paper)	68	65	67	53

142 Projection of future ozone concentrations by CTM simulation under assumptions regarding the temporal evolution
 143 of ozone precursor emissions and other relevant model parameters has provided a widely utilized tool for air quality
 144 policy development. Such projections have also been made by our observational-based model under assumed future
 145 evolution of the background and anthropogenic ozone contributions; here the parameterized temporal evolution of
 146 each contribution over the past decades was assumed to continue into the future. Parrish et al. (2017) made such ODV
 147 projections for seven southern CA air basins (their Figure 8, a portion of which is reproduced here). Those projections
 148 can now be compared with 8 years of ODVs that have been recorded
 149 since the projections were made; they are included in the figure to
 150 the right of the vertical dashed line. The projections had only mixed
 151 success; there is good agreement with the recent ODVs in the two,

Original Figure 8 of Parrish et al. (2017). Past and projected evolution of the basin ODVs in southern California air basins. The symbols give the annual ODVs for each air basin, and the solid curves indicate the fits of their Equation 1, with the parameters from their Table 4, to the corresponding ODVs with projections to the year 2058. The horizontal dashed line indicates the NAAQS. **Added here:** Eight more recent years of ODVs are included for each of the 4 coastal air basins; they lie to the right of the vertical dashed line. The results for the 3 inland air basins have been removed for clarity. The larger asterisk symbols indicate CTM-derived ODV projections for the two more urbanized air basins

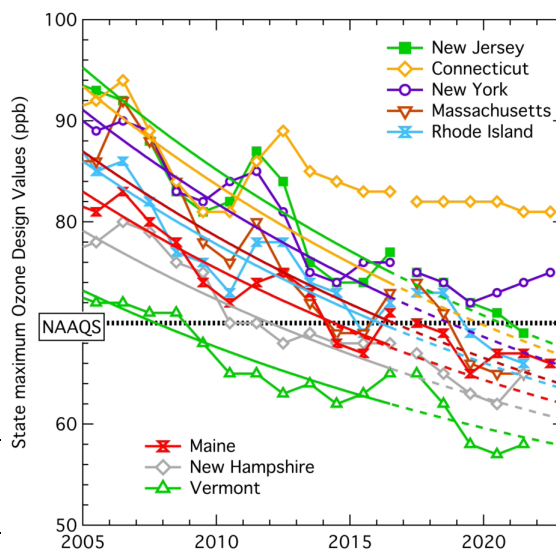


152 less urbanized (North and South Central Coast) air basins, but the projections did not capture the observed increases
 153 of the recent ODVs in the more urbanized San Diego and South Coast air basins. However, in these two air basins,
 154 the CTM predictions (indicated in the figure) were even less accurate. The California Air Resources Board (CARB,
 155 2019) staff report for the Southern California AB predicted that the ODV would be 80 ppb by 2023, some 26 ppb
 156 below the observed value of 106 ppb, while the Parrish et al. (2017) projection was found to be too low as well, but
 157 at 90 ppb was 10 ppb closer than the CTM. For the San Diego AB the CARB (2017) staff report predicted that the
 158 ODV would fall to 75 ppb in the year 2017, Parrish et al. (2017) projected 78 ppb, while 84 ppb was actually recorded.
 159 The cause of the unexpected increases in the urbanized air basins remains largely unexplained (Wu et al., 2023).

160 Parrish and Ennis (2019) projected maximum ODVs in eight northeastern US states (dashed curves in an expanded
 161 portion of their Figure 10 reproduced below) following the last year with ODVs available to them (2017). Here we
 162 evaluate the fidelity of those projections. For our analysis, ODVs from 2018-2022 or 2023 (depending on the state)
 163 had become available; we have added those ODV symbols to the figure shown here. Most of the more recent ODVs
 164 agree well with the projections, but in two states (Connecticut and New York) they deviate noticeably. These
 165 deviations are due to ODVs from coastal sites on the Long Island Sound, not from the major urban centers in the
 166 states. This suggests that photochemical ozone production from precursors trapped within the shallow marine
 167 inversion layer significantly impact maximum ozone concentrations in air transported ashore to these sites. Insights
 168 such as this make simple observation-based models particularly useful. Parrish and Ennis (2019) also projected the
 169 year in which ODVs would drop to the NAAQS (their table reproduced below). We have added a final column to that
 170 table indicating when the ODVs actually reached that limit. Again, with the exception of the same two states,
 171 reasonable agreement between the projections and reality is found, especially when the 2 to 4 ppb RMSD of the ODVs
 172 about the fits are considered. Projections of the future
 173 development of ODVs from our model can provide policy
 174 relevant information, although (as with any model projection)
 175 that information must be carefully evaluated.

Original Table 3 of Parrish and Ennis (2019). Results of least-squares fits of Equation 1 to the state maximum ODVs illustrated Figure 10; y_0 and τ were held constant at 45.8 ppb and 21.9 years, respectively. The absolute root-mean-square deviations between the observed ODVs and the derived fits are indicated. Year_{NAAQS} indicates the projected year that the fit to the state maximum ODV drops to the NAAQS of 70 ppb. **Column added here:** Last year of recorded ODV \geq NAAQS.

State	A^* (ppb)	RMSD (ppb)	Year _{NAAQS}	Last year ODV \geq NAAQS
Connecticut	61 ± 7	5.8	2021	>2023
Maine	48 ± 4	3.2	2015	2010
Massachusetts	53 ± 5	3.9	2017	2019
New Hampshire	43 ± 4	3.0	2013	2012
New Jersey	64 ± 5	3.7	2021	2022
New York	58 ± 4	3.0	2019	>2023
Rhode Island	52 ± 4	3.4	2017	2019
Vermont	35 ± 3	2.1	2008	2009



Original Figure 10 of Parrish and Ennis (2019). Time series of maximum ODVs reported from any site within each of the eight northeastern states. The solid curves are fits of Equation 1 to the respective colored symbols for the 2000-2017 period. The derived A^* values from these latter fits are given in Table 3. The dashed lines are projections of the solid curves. **Added here:** 5 or 6 more recent years of ODVs are included in each state.

176 **S2. Relationship of US background ODV to ozone exceedance days**

177 (Note: A previous version of some of this material was originally included in the Supplement to Parrish et al., 2022 -
178 <https://www.tandfonline.com/doi/suppl/10.1080/10962247.2022.2050962?scroll=top&role=tab>)

179 One important question lacks a definitive answer: Are the four days that record the highest MDA8 ozone
180 concentrations, i.e., the days that determine the ODV at present, the same four days that correspond to the highest US
181 background, i.e., the days that would determine the ODV in the absence of anthropogenic precursor emissions? In
182 other words, do the present highest ozone days also correspond to the days with the largest background ozone?
183 Photochemical models provide a direct answer, but given the uncertainty associated with modeled background ozone
184 concentrations on specific days (estimated as >10 ppb by Jaffe et al., 2018) this answer is likely not reliable. From our
185 observational perspective, we cannot directly answer this question; however observation-based analyses can
186 illuminate this question. It is useful to consider a heuristic example based on artificial data that illustrates some
187 important considerations when considering this issue.

188 Figure S7 represents an imaginary world that has no meteorological variability; every day is exactly like every
189 other, except that there are gradual seasonal changes. The upper graph shows how MDA8 ozone might vary seasonally
190 at a particular measurement site (black curves decreasing in amplitude over time due to emission controls.) With no
191 US anthropogenic precursor emissions, ozone would equal the US background ozone (blue curve, assumed to average
192 40 ppb with a sinusoidal variation of 20 ppb amplitude), and would vary smoothly over the year, repeating identically
193 each year. The US background ODV (i.e., the quantity we estimate in our work, which here is assumed constant)
194 would then be given by the blue symbol very near the peak of the blue curve.

195 US anthropogenic ozone precursor emissions in 2000 are assumed to increase the background ozone by an amount
196 given by the red curve (average 35 ppb with a sinusoidal variation of 40 ppb amplitude). The blue and red curves are
197 3 months out of phase, in approximate accord with observed Northern Hemisphere background free-tropospheric
198 ozone concentrations that peak in the spring (April/May) and many urban areas that peak in mid to late summer. The
199 total ozone measured in 2000 would then be given by the highest black curve, and the site ODV given by the highest
200 black symbol. Subtraction of the US background ODV from the site ODV gives the US anthropogenic ODV
201 enhancement in 2000 as indicated by the red arrow. Notably, that quantity (60 ppb) is smaller than the US
202 anthropogenic contribution to the ODV in 2000 (~71 ppb, given by orange arrow). This illustration lies at the heart of
203 a common misunderstanding: the US background ODVs reported in this work are not the same as the current
204 contributions of background ozone to current ODVs, because the maxima of background ozone and anthropogenic
205 enhancements are offset from each other in the time of year when they occur. Nevertheless, when considering progress
206 in reducing US anthropogenic precursor emissions, the US background ODV is still germane for considerations of
207 compliance with the NAAQS.
208

209 Now we assume that the US anthropogenic
 210 ozone production decreases exponentially with a
 211 time constant of 20 years. Consequently, the total
 212 measured ozone (black curves) decreases year-by-
 213 year, with the ODVs (black symbols) also
 214 decreasing, and simultaneously shifting to earlier in
 215 the year, and approaching the US background ODV
 216 (i.e., the blue symbol).

217 As shown in the lower graph of Figure S7, the
 218 changes in site ODVs (black symbols in both
 219 graphs) are well fit by an exponential decay, as
 220 given by Equation 3 of the manuscript. The derived
 221 parameter $a = 60.0 \pm 0.4$ ppb agrees with the 60 ppb
 222 maximum of the blue curve, and the parameter $A =$
 223 59.8 ± 0.3 ppb agrees with the 60 ppb magnitude of
 224 the year 2000 US anthropogenic ODV enhancement
 225 (red arrow in figure).

226 An important conclusion from this illustrative
 227 example is that confusion can arise if a clear
 228 distinction is not made between the US
 229 anthropogenic ODV enhancement in 2000 (i.e., the
 230 red arrow), the anthropogenic contribution to the
 231 site ODV (i.e., the orange arrow) and the
 232 anthropogenic ozone production (i.e., the red curve,
 233 which varies during the year).

234 One implication of this example is that episode
 235 days (i.e., those exhibiting the highest ozone) in
 236 earlier decades are not seasonally coincident with
 237 present episode days, and neither of those sets of
 238 episode days is seasonally coincident with future
 239 episode days. This is due to the growing relative
 240 importance of background ozone (which is larger in
 241 spring and early summer) as the magnitude of local
 242 and regional photochemical production, which is
 243 larger later in the summer, decreases. In actuality, episode days in southern California air basins have been observed
 244 to systematically move toward the spring from later in the summer; Parrish et al. (2017) show that when monitoring
 245 began in the South Coast Air Basin of California (i.e., the Los Angeles urban area) in the early 1970s, the average
 246 ozone episode day occurred in late July, but had progressively moved to early July by 2015. This seasonal shift of

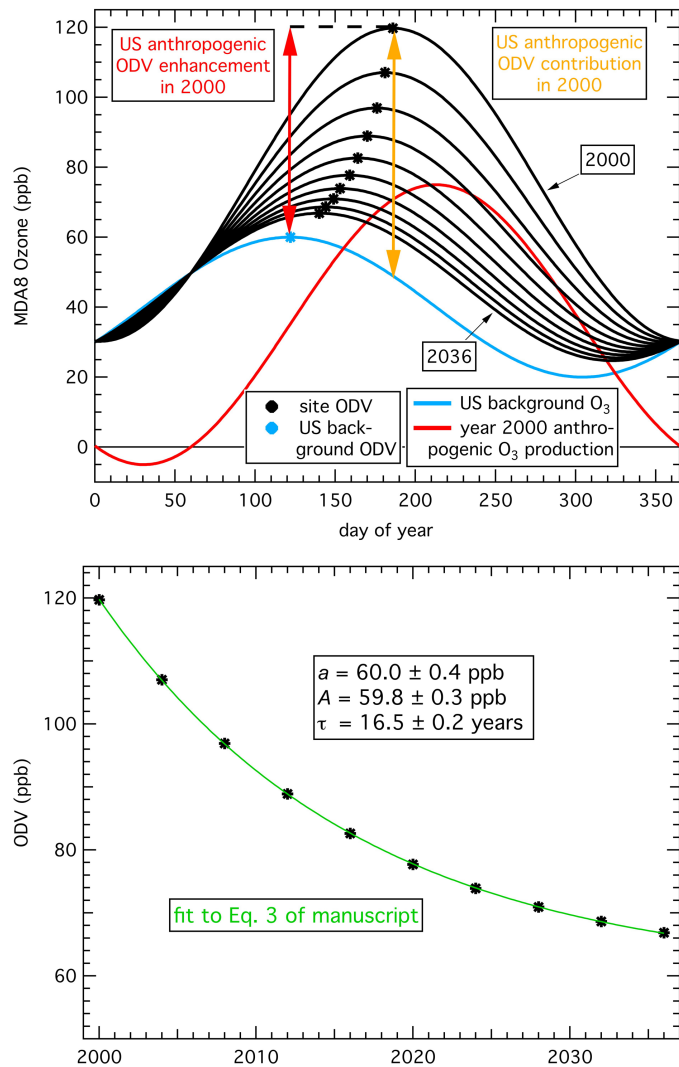


Figure S7: Schematic variation of ozone at a measurement site. **(top)** Blue and red curves give the assumed constant US background ozone and the US anthropogenic ozone production in the year 2000, respectively. The black curves are the total observed ozone in the year 2000 and at progressively later 4-year intervals. The US background ODV is given by the blue symbol, and the site ODVs are given by the black symbols at the peak of their respective curves. The year 2000 US anthropogenic ODV enhancement and anthropogenic ODV contribution are given by the red and orange arrows, respectively. **(bottom)** Temporal evolution of site ODVs from upper graph, fit to Equation 3 of the manuscript, with derived parameters annotated.

247 episode days adds considerable uncertainty to photochemical modeling for State Implementation Plan (SIP)
248 development. The meteorological conditions (including the background ozone contribution) on the days that will
249 require the greatest emission control efforts to lower the MDA8 ozone to the NAAQS is uncertain. The common
250 assumption that those days correspond to the present maximum episode days is not valid, since days with higher
251 background ozone concentrations may require even greater emission reductions to reach the NAAQS, even if they
252 now are not the days when the highest ozone is observed.

253 It should also be noted that an observation-based analysis has indicated a significant positive correlation between
254 maximum observed ozone concentrations and high background ozone concentrations. Parrish et al. (2010) show that
255 MDA8 ozone measured at surface sites in California's Northern Sacramento Valley correlates positively (correlation
256 coefficients as large as +0.53 at valley sites and +0.71 at an elevated surface site) with baseline ozone concentrations
257 measured by sondes launched from the upwind location at Trinidad Head on the northern California coast. This
258 analysis suggests that the days that determine the ODV will progressively tend to be the days of highest US background
259 ozone concentration as anthropogenic ozone contributions are further reduced.

260 It has been argued (e.g., see Section 1.8 of US EPA, 2020) that the highest US ozone concentrations occur during
261 periods of low background ozone contributions. This argument is based on the reasoning that the largest background
262 ozone contributions occur on spring days with strong convective mixing when ozone generated in the stratosphere or
263 during long-range transport of Asian or natural precursors in the upper troposphere are more readily mixed to the
264 surface. In contrast, the highest US ozone concentrations are thought to occur during multiday episodes under stagnant
265 conditions when an air mass remains stationary over a region abundant in anthropogenic ozone precursor sources.
266 However, this reasoning does not apply to the southwestern US, because surface ozone concentrations are strongly
267 correlated with higher ambient temperatures, and higher temperatures are correlated with deeper atmospheric
268 boundary layers (ABL) in this area. Examination of the climatology of ABL heights over western North America
269 shows that in summer, when most ozone NAAQS violations occur, boundary layers tend to be deepest (see figure 5
270 of von Engel and Teixeira, 2013). Deeper boundary layers develop due to greater vertical mixing driven by strong
271 surface heating (i.e., entrainment). A recent paper (Langford et al., 2022) emphasizes that layers with elevated ozone
272 concentrations above Las Vegas were commonly entrained into the ABL and thereby contributed to mean MDA8
273 regional background ozone concentrations of 50–55 ppb; note that our paper analyzes ODVs, which represent ~98th
274 percentile MDA8 concentrations, and, as expected, the US background ODVs that we quantify are substantially larger
275 than the 50–55 ppb mean background ozone discussed by Langford et al. (2022).

276 Photochemical modeling in support of air quality policy development has generally focused on days exhibiting
277 the largest MDA8 ozone concentrations. This choice is based on the implicit assumption that such days represent the
278 meteorological conditions under which it will be most difficult to reduce the MDA8 to the NAAQS. Importantly, the
279 US background ODV that is the focus of our analysis may not occur on those same days. Photochemical modeling
280 on days with larger US background ODVs will be very informative, but such days are difficult to specifically
281 identify.

282 S3. Approximation of long-term change of US anthropogenic ODV enhancements by an exponential decrease

283 An exponential function is chosen to approximate the long-term decrease of US anthropogenic ODV enhancements
284 because it a) is consistent with our physical understanding of the drivers of urban and rural ozone concentrations, b)
285 is a continuous function, c) is mathematically as simple as possible (i.e., has the fewest possible unknown parameters),
286 and d) successfully accounts for a large fraction of the variance in recorded ODV time series throughout the US.

287 Any functional form selected for interpretation of an ODV time series must be consistent, first, with a background
288 contribution below which ODVs cannot be reduced by U.S. precursor emission controls alone, and second, with ODVs
289 that have been enhanced above that background due to a pollution contribution, an enhancement that has continually
290 decreased due to decades-long precursor emission reduction efforts. Equation 3 of the manuscript is designed to follow
291 this physical picture. More generally, examination of ozone observations in US urban areas reveals similar trends
292 throughout the country, with general decreases in all areas. A simple intuitive argument suggests that an exponential
293 decrease in the pollution ozone contribution is to be expected. When emission controls are initiated, early progress
294 can be rapid, since there are large emission sources that evolved initially with no plans for their control. As an
295 illustrative example, when emission controls are first initiated it might be possible to reduce the pollution ozone
296 contribution by half in the first 15 years of control efforts. After that period reducing emissions will be harder, since
297 the most easily controlled emissions have been addressed. During the next 15 years, it might be possible to again
298 reduce the remaining pollution ozone contribution by half (i.e., reduction of 25% of the original). A similar argument
299 can be applied to each successive 15-year period. If this example were realistic, then the emission reductions would
300 follow an exponential function, with $\tau = 21.6$ years, close to the value of $\tau = 21.8 \pm 0.8$ years reported by Parrish et
301 al. (2022). Simply put, the expected increasing difficulty of reducing emissions by an absolute amount implies an
302 approximately exponential decrease in the impact of those emissions.

303 Despite the large variability of tropospheric ozone on a wide spectrum of temporal scales, the underlying long-
304 term changes in ODVs are expected to be continuous, since they are determined by slowly varying drivers such as
305 changes in anthropogenic precursor emissions, land use (which affects natural precursor emissions), and climate.
306 Exceptions might include rapid societal changes, such as occurred during the COVID-19 epidemic response, and
307 volcanic eruptions; however, no discontinuous long-term changes have been encountered in all of the US ODV time
308 series we have analyzed. Thus, the choice of the exponential function, which is continuous, is again indicated.

309 The exponential term of Equation 3 - $A \exp(-t/\tau)$ - with two parameters is the simplest possible functional form
310 that can capture the behavior of the pollution enhancement. Each ODV is a three-year average; hence a three-decade
311 ODV time series provides only 10 independent data. The ODVs have significant short-term variability (e.g., Guo et
312 al., 2018), so an attempt to quantify systematic, long-term changes from available ODV time series requires fitting
313 to no more than a simple mathematical function for that quantification. That is, to yield precise determinations of the
314 values of the function's parameters the function must have as few unknown parameters as possible. A linear
315 function, also with two parameters - slope and intercept - is often utilized for time series fits; it is as mathematically
316 simple as an exponential function, but a linear fit to a decreasing trend will eventually become negative, and
317 therefore cannot generally be consistent with a positive background contribution. A linear decrease that ends when it
318 intersects a background function, such as a constant or the function given by the first three terms of Equations 3 and

319 4 of the manuscript, requires only two parameters, but the resulting function is not continuous. Likewise, piece-wise
320 linear fits are not continuous, and generally require at least four parameters to specify. Any other function that might
321 be applied (e.g., a polynomial fit) would require more than two parameters. From a simplicity and continuity
322 perspective, the chosen exponential function is uniquely suited for quantifying a decreasing ODV time series.

323 Finally, experience has shown that an exponential function gives excellent fits to the last two to five decades of
324 ozone observed in US urban areas. In their section 2.4 Parrish et al. (2017) present a multivariate fit of Equation 3
325 (but with a constant background term) to maximum ODV time series in seven southern California air basins over 35
326 years; the r^2 value for that fit is 0.984. In a similar analysis Parrish and Ennis (2019) find an r^2 value of 0.89 for a
327 shorter (17 year) period of time series of maximum ODVs recorded in eight northeastern states. Section S6 below
328 discusses similar analyses for ODV time series analyzed in this manuscript, and again find large r^2 values – 0.94 for
329 eight Texas regions and 0.79 for the maximum ODV time series in eight southwestern US urban areas. These large
330 r^2 values demonstrate that an exponential function accurately captures a large fraction (approximately equal to the
331 respective r^2 values) of the variance in the ODV time series in all US regions that we have investigated. These
332 considerations demonstrate that an exponential function is a very effective choice for analysis of long-term ozone
333 time series.

334 **S4. Differing rates of decrease of anthropogenic precursor emissions are not directly treated**

335 Equation 3 includes only a single term to account for the influence of decreasing anthropogenic emissions on ODVs;
336 that term depends on a single exponential time constant, τ . However, different anthropogenic emission sectors may
337 have differing time evolution of emissions, which may be expected to be reflected in the temporal evolution of ODVs.
338 In effect, τ in Equation 3 is assumed to represent an average, overall response of ODVs to decreasing anthropogenic
339 emissions.

340 In this and previous work we discuss the impact of two anthropogenic emission sectors that have not decreased.
341 First, southern California has regions of very intensive agricultural activity - the Imperial Valley in the Salton Sea Air
342 Basin, the San Joaquin Valley Air Basin, and the Salinas Valley in the North Central Coast Air Basin; Parrish et al.
343 (2017; 2022) note that derived a parameter values are biased high by ~ 5 to 12 ppb in these locations, and thus cannot
344 be interpreted as direct determinations of the US background ODV. Second, the development of Equation 4 provides
345 an approximate treatment of the increasing influence of wildfires on ODVs; a small wildfire influence (WF up to 4
346 ppb) could be discerned in the region studied in this work, and a larger influence (~ 10 -15 ppb) was approximately
347 quantified in urban areas of the Pacific Northwest (Parrish et al., 2022).

348 There are additional anthropogenic emission sectors that may not have decreased over time, and hence could
349 possibly bias our estimate of US background ODVs. These sources include emissions associated with oil and gas
350 (O&G) exploration, drilling and production, which have increased over the past two decades in some regions of the
351 Western US. In addition, nonroad equipment, such as construction equipment, lawn and garden equipment, and VCP
352 emissions (Coggon et al., 2021) may be important in urban areas, and they have not received as much regulatory
353 attention as anthropogenic emissions. The Supplement Section S5 of Parrish et al. (2022) analyzes time series of ozone
354 observations in the Bakken O&G basin located in North Dakota, and examines correlations of derived a and A

355 parameter values in West Coast urban areas. That discussion found no indications of a significant bias arising from
356 these emissions sectors.

357 **S5. Value of exponential decrease time constant, τ , determined in Southern California, applied to the entire** 358 **southwestern US**

359 We have not found it possible to precisely determine the three parameters (a , A and τ) of Equation 3 from a fit to
360 most available US ODV time series. The analysis in the manuscript assumes that τ in the southwestern US and
361 Texas (as well as other states considered) is the same value as derived for southern California ($\tau = 21.8 \pm 0.8$ years).
362 This assumption follows from the perspective of other states closely following the lead of California in emission
363 control efforts, and is supported by the excellent fits provided by Equation 3 to ODV time series throughout the US,
364 as discussed above in Section S4.

365 Generally, it is not possible to precisely determine the three parameters (a , A and τ) of Equation 3 from a fit to
366 most available US ODV time series. Here, however we conduct two iterative, multivariate regression analyses,
367 similar to that described in Section 2.4 of Parrish et al. (2017) and applied by Parrish and Ennis (2019) to the
368 northeastern US. Simultaneous fits to several ODV time series improve the precision of the parameter
369 determinations, allow alternate derivation of some parameter values, and provide alternate estimates of confidence
370 limits for the derived parameter values. Two separate analyses, each analyzing eight ODV time series, are presented.
371 The first analysis fits Equation 3 to ODV time series from the first eight Texas regions listed in Table S5 and
372 illustrated in Figures 8 and S4; the western rural region is omitted due to its small range of recorded ODVs. An
373 ODV time series for each region is obtained by averaging all ODVs collected in that region for each year of the
374 temporal ranges indicated in Table S5. A separate exponential time constant, τ_{Ho} , is derived for the Houston region,
375 and a single parameter value for τ is derived for the other seven regions. Values of these two τ values and 16 total
376 separate a and A parameter values for each of the eight regions are optimized in an iterative process that minimizes
377 the sum of the squares of the deviations between the fit and the original mean ODV time series. The second analysis
378 fits Equation 4 to the maximum ODV time series in the seven southwestern US urban areas discussed in Section 4.3
379 and plotted as light red solid circles in Figures 5 and 6, and the maximum El Paso ODV time series plotted in Figure
380 8. A similar iterative process attempts to optimize single common parameter values for τ and the wildfire
381 proportionality constant (i.e., the factor of 0.03 in Equation 4) for all areas, and separate a and A parameter values of
382 each of the eight regions. For both analyses the 18 derived parameter values are given in Table S8, and Figure S8
383 compares the fits of Equations 3 and 4 to the original ODV time series, both for the original fits discussed in the
384 manuscript (upper graphs) and for the multivariate analyses (lower graphs).

385 The three derived τ values (18.4 to 19.1 years) are up to 16% smaller than the southern California value of $21.8 \pm$
386 0.8 years, and are outside the 95% confidence limit of the California value. However, it is very difficult to force
387 convergence of the Texas multivariate fit, and not possible for the southwestern US analysis due to anti-correlations
388 between parameters. Notably, the agreement between the a and A parameter values between the original analysis
389 (assuming derived $\tau = 21.8 \pm 0.8$ years) and the multivariate analysis (83% overall) is usually within the confidence
390 limits of the original analysis, and these multivariate fits provided only very modest improvements over the original

391 fits in the overall r^2 and RMSD values (compare final two rows in Table S8). Given this overall agreement, we are
 392 confident in our application of the southern California value of τ throughout the entire region studied in this work.

393 **Table S8.** Parameter values derived from multi-variate fits described in Section S3. All units are ppb ozone unless
 394 otherwise noted, except for the dimensionless parameter, r^2 .

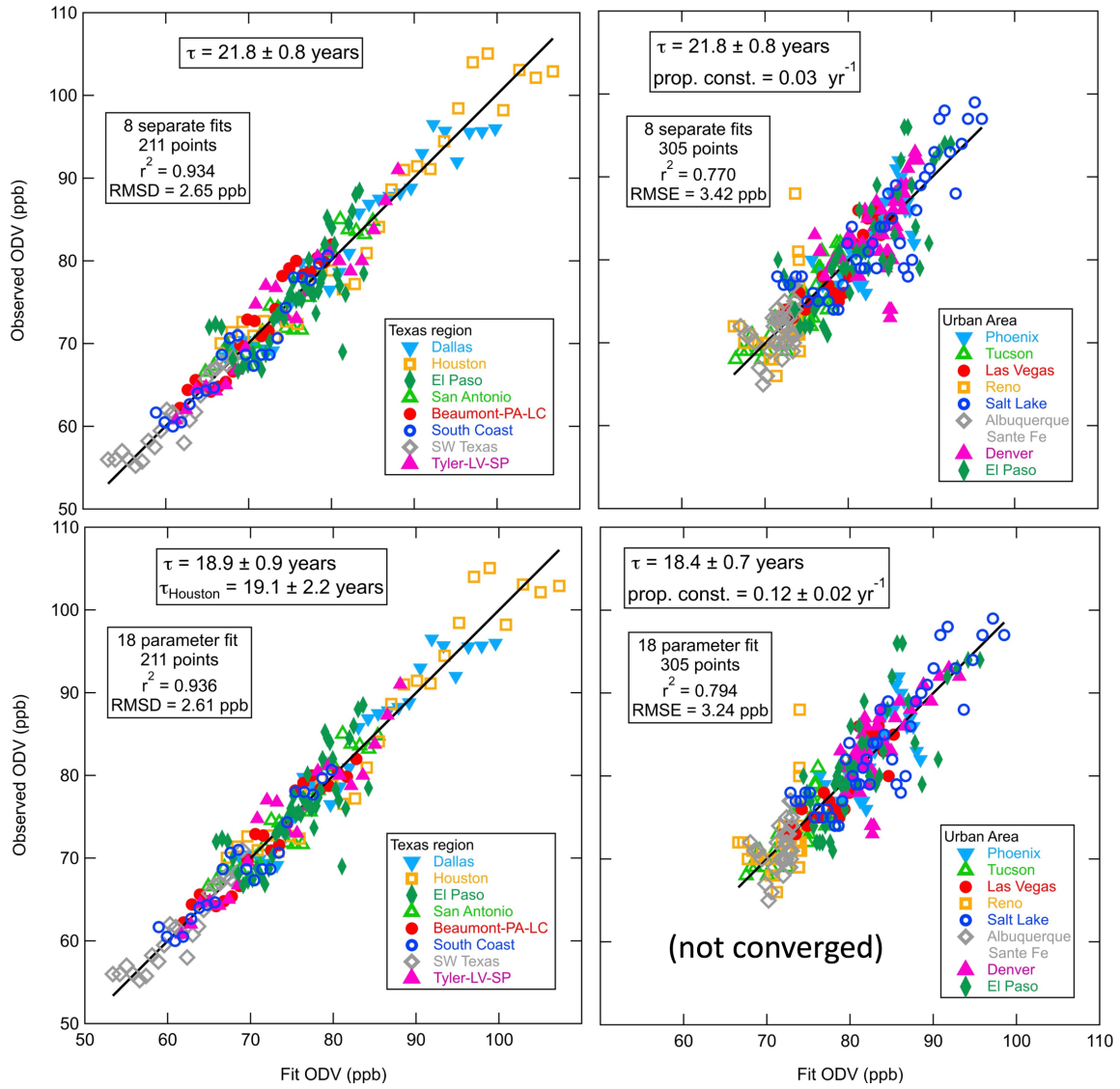
Texas region	Original fits ^a	Multi-var fit	SW US urban area	Original fits ^b	Multi-var fit ^c
τ (years)	21.8 ± 0.8	18.9 ± 0.9	τ (years)	21.8 ± 0.8	18.4 ± 0.7
τ_{Ho} (years)	21.8 ± 0.8	19.1 ± 2.2	prop. const. (year ⁻¹)	0.03	0.116 ± 0.19
Dallas - <i>A</i>	34.6 ± 4.5	30.3 ± 1.7	Phoenix - <i>A_{WF}</i>	12.9 ± 3.6	12.8 ± 1.9
Dallas - <i>a</i>	57.7 ± 3.1	61.6 ± 1.3	Phoenix - <i>a</i>	69.0 ± 1.7	70.5 ± 1.7
Houston - <i>A</i>	43.2 ± 4.2	39.1 ± 1.7	Tucson - <i>A_{WF}</i>	10.5 ± 1.6	10.6 ± 1.3
Houston - <i>a</i>	53.9 ± 3.2	57.9 ± 1.3	Tucson - <i>a</i>	63.9 ± 1.4	63.1 ± 1.6
El Paso - <i>A</i>	11.5 ± 1.7	9.2 ± 0.6	Las Vegas - <i>A_{WF}</i>	16.1 ± 6.6	16.8 ± 3.3
El Paso - <i>a</i>	64.6 ± 1.8	66.6 ± 1.0	Las Vegas - <i>a</i>	68.0 ± 2.6	67.6 ± 2.1
San Antonio - <i>A</i>	26.6 ± 6.3	25.0 ± 2.2	Reno - <i>A_{WF}</i>	7.0 ± 1.3	6.8 ± 1.2
San Antonio - <i>a</i>	58.4 ± 4.1	60.4 ± 1.4	Reno - <i>a</i>	66.3 ± 2.2	66.1 ± 1.6
Beau.-PA-LC - <i>A</i>	28.0 ± 5.1	25.5 ± 2.2	Salt Lake City - <i>A_{WF}</i>	15.6 ± 2.0	14.9 ± 1.0
Beau.-PA-LC - <i>a</i>	54.7 ± 3.4	57.2 ± 1.4	Salt Lake City - <i>a</i>	66.6 ± 1.9	66.3 ± 1.5
So Coast Texas - <i>A</i>	27.5 ± 6.0	25.6 ± 2.2	Albuquer.-SF - <i>A_{WF}</i>	6.0 ± 1.5	6.9 ± 1.1
So Coast Texas - <i>a</i>	52.1 ± 4.1	54.2 ± 1.4	Albuquer.-SF - <i>a</i>	66.2 ± 1.8	64.7 ± 1.5
SW Texas - <i>A</i>	18.2 ± 6.9	16.7 ± 2.1	Denver - <i>A_{WF}</i>	11.0 ± 1.7	13.4 ± 0.8
SW Texas - <i>a</i>	49.8 ± 4.9	51.6 ± 1.4	Denver - <i>a</i>	69.0 ± 2.1	64.5 ± 1.5
Tyler-LV-SP - <i>A</i>	37.3 ± 6.8	33.8 ± 2.2	El Paso - <i>A_{WF}</i>	14.2 ± 2.1	15.1 ± 0.9
Tyler-LV-SP - <i>a</i>	50.8 ± 4.6	54.2 ± 1.4	El Paso - <i>a</i>	64.6 ± 1.8	62.3 ± 1.5
r^2 ^d	0.934	0.936	r^2 ^d	0.770	0.794
RMSD ^d	2.65	2.61	RMSD ^d	3.42	3.24

395 ^a Fits described in Section 4 of the paper. Values are reproduced from Table S5.

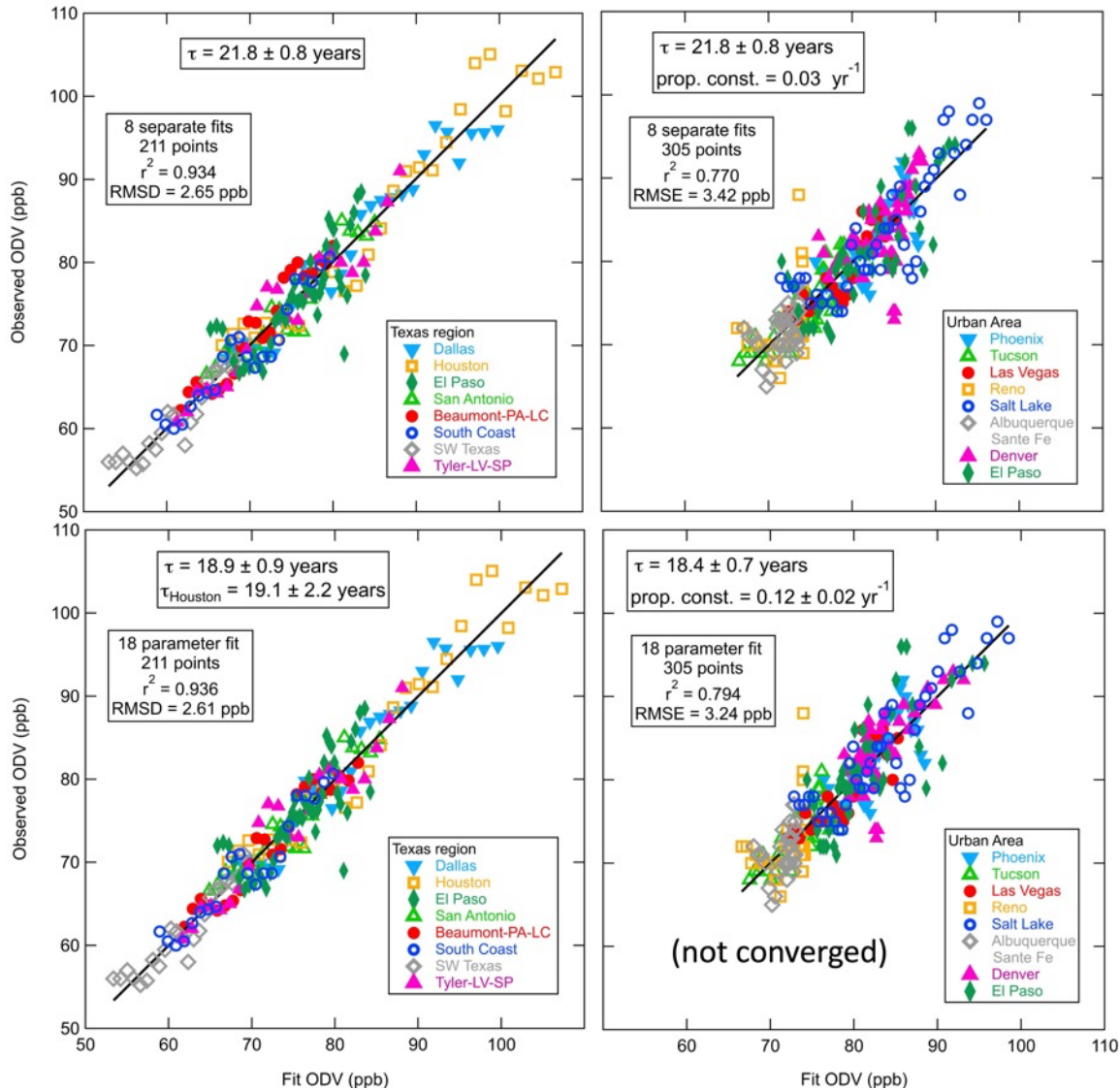
396 ^b Fits described in Section 4 of the paper. Values are reproduced from Tables S3 and S4.

397 ^c Multivariate fit did not converge; these results were obtained after a large number of iterations of the fitting
 398 routine.

399 ^d r^2 and RMSD are the parameters for the linear regression fit between the actual ODVs and the fit function, as
 400 shown in Figure S8.



401



402

403 **Figure S8.** Comparison of observed ODVs with those from fits. The Texas regional and southwestern US urban
 404 time series are on the left and right, respectively. The fits to individual time series from the paper are at the top and
 405 the simultaneous multivariate fits to all of the time series are at the bottom. Black lines give the linear fit to all points
 406 with the intercept held at zero; the slopes of all lines are within 0.0013 of unity, the value expected for a perfect fit.
 407 The iterative process was not able to locate a unique minimum for the sum of the squares of the deviations for the 18
 408 parameter fit to the southwestern US urban time series; this is attributed to poor constraints on all 18 parameters in
 409 the that data set.

410 S6. Effect of not considering the US Exceptional Event Rule

411 In this work we utilize the ODVs tabulated in the data archive of the US EPA to quantify the maximum ozone
 412 concentrations impacting surface monitoring sites, and to determine whether a site is approaching or exceeding the
 413 NAAQS. It should be noted that if measurement data are influenced by exceptional events, such as wildfires (e.g.,

414 Jaffe et al., 2013) or stratospheric ozone intrusions (e.g., Langford et al., 2017), those data can, in principle, be
415 removed from the MDA8 monitoring record, as uncontrollable “exceptional events”, thereby affecting the ODV
416 archive. More details of the Exceptional Events Rule can be found on the US EPA website: [https://www.epa.gov/air-](https://www.epa.gov/air-quality-analysis/treatment-air-quality-data-influenced-exceptional-events-homepage-exceptional)
417 [quality-analysis/treatment-air-quality-data-influenced-exceptional-events-homepage-exceptional](https://www.epa.gov/air-quality-analysis/treatment-air-quality-data-influenced-exceptional-events-homepage-exceptional). If a significant
418 number of ODVs were affected by excluded data, then the ODV archive would not faithfully reflect the actual time
419 series of maximum ozone concentrations, or the true relationship of the ozone concentrations at a site to the
420 NAAQS. Data are excluded when the US EPA concurs with a state’s exceptional event demonstration.

421 The US EPA apparently does not maintain a data base of exceptional event concurrences, but so far as we can
422 determine from an internet search, at the time of this writing, the US EPA has concurred with only one ozone
423 exceptional event demonstration in the five southwestern US states plus TX and CA examined in this paper since the
424 implementation of the 2016 Exceptional Events Rule. That event was on September 2 and 4, 2017 when wildfires in
425 the Pacific Northwest impacted the National Renewable Energy Laboratory (NREL) ozone monitoring site operated
426 in the greater Denver urban area. As a result of this concurrence the ODV at that site would be reduced by 1 ppb for
427 the years 2017 (from 80 to 79 ppb) and 2019 (from 77 to 76 ppb). In 2017, but not in 2019, this site recorded the
428 maximum ODV in the Denver area, so the urban maximum ODV would be reduced by 1 ppb in 2017, but not
429 affected in 2019. According to the statistics compiled by David et al. (2021), there were 5 other exceptional events
430 totalling 14 days to which the EPA concurred in 2000-2015 under an earlier exceptional event rule; thus, there has
431 been on average only 1 exceptional event every 3 years successfully removed from nonattainment consideration
432 within the seven state region.

433 In summary, archived ODVs can be reduced by US EPA exceptional event concurrences; however, to date
434 concurrences have been extremely limited, and therefore have not significantly affected the analysis presented in
435 this paper. However, future concurrences may possibly affect application of the present analysis approach to coming
436 years.

437 **References not included in manuscript**

- 438 California Air Resources Board, ARB Review of the 2008 8-Hour Ozone Attainment Plan for San Diego County,
439 Release Date: February 17, 2017. [https://ww2.arb.ca.gov/our-work/programs/california-state-implementation-](https://ww2.arb.ca.gov/our-work/programs/california-state-implementation-plans/nonattainment-area-plans/san-diego-county)
440 [plans/nonattainment-area-plans/san-diego-county](https://ww2.arb.ca.gov/our-work/programs/california-state-implementation-plans/nonattainment-area-plans/san-diego-county).
- 441 California Air Resources Board, South Coast 8-Hour Ozone SIP Update, Release Date: November 8, 2019.
442 <https://ww2.arb.ca.gov/resources/documents/2019-south-coast-8-hour-ozone-sip-update>.
- 443 Coggon, M. M., Gkatzelis, G. I., McDonald, B. C., Gilman, J. B., Schwantes, R. H., Abuhassan, N., Aikin, K. C.,
444 Arend, M. F., Berkoff, T. A., Brown, S. S., et al.: Volatile chemical product emissions enhance ozone and
445 modulate urban chemistry, *Proceedings of the National Academy of Sciences* 118 (32):e2026653118.
446 doi:10.1073/pnas.2026653118, 2021.
- 447 David, L. M., Ravishankara, A. R., Brey, S. J., Fischer, E. V., Volckens, J. and Kreidenweis, S.: Could the exception
448 become the rule? ‘Uncontrollable’ air pollution events in the US due to wildland fires. *Environmental Research*
449 *Letters* 16, no. 3, 034029, 2021.

450 Guo, J.J., Fiore, A.M., Murray, L.T., Jaffe, D.A., Schnell, J.L., Moore, C.T., and Milly, G.P.: Average versus high
451 surface ozone levels over the continental USA: model bias, background influences, and interannual variability,
452 *Atmos. Chem. Phys.*, 18, 12123–12140, doi.org/10.5194/acp-18-12123-2018, 2018.

453 Jaffe, D., Wigder, N., Downey, N., Pfister, G., Boynard, A., and Reid, S. B.: Impact of Wildfires on Ozone
454 Exceptional Events in the Western US, *Environ. Sci. Technol.*, 47, 11065–11072,
455 <https://doi.org/10.1021/es402164f>, 2013.

456 Kaldunski, B., Pierce, R. B., and Holloway, T.: When Stratospheric Ozone Hits Ground-level Regulation:
457 Exceptional Events in Wyoming *Bull. Am. Meteorol. Soc.*, 98(5), 889-892, doi:10.1175/BAMS-D-14-00133.1,
458 2017.

459 Parrish, D. D., Aikin, K. C., Oltmans, S. J., Johnson, B. J., Ives M., and Sweeny, C.: Impact of transported
460 background ozone inflow on summertime air quality in a California ozone exceedance area, *Atmos. Chem.*
461 *Phys.*, 10, 10093–10109, doi:10.5194/acp-10-10093-2010, 2010.

462 State of Wyoming: Exceptional Event Demonstration Package for the Environmental Protection Agency: Big Piney
463 and Boulder, Wyoming Ozone Standard Exceedances June 14, 2012, edited, Department of Environmental
464 Quality/Air Quality Division, 2013.

465 US EPA: Integrated Science Assessment (ISA) for Ozone and Related Photochemical Oxidants (Final Report, Apr
466 2020). U.S. Environmental Protection Agency, Washington, DC, EPA/600/R-20/012, 2020.

467 von Engel, A., and Teixeira, J.: A Planetary Boundary Layer Height Climatology Derived from ECMWF
468 Reanalysis Data, *J. of Climate*, 26(17), 6575–6590, <https://doi.org/10.1175/JCLI-D-12-00385.1>, 2013.

469 Wu, K., Zhu, S., Mac Kinnon, M., and Samuelsen, S.: Unexpected deterioration of O₃ pollution in the South Coast
470 Air Basin of California: The role of meteorology and emissions. *Environmental Pollution*, 330, 121728, 2023.